Chemical Geology 616 (2023) 121222

Contents lists available at ScienceDirect

Chemical Geology

journal homepage: www.elsevier.com/locate/chemgeo

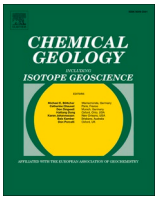

Mineral precipitation and hydrochemical evolution through evaporitic processes in soda brines (East African Rift Valley)

Melese Getenet [a], Fermín Otálora [a], Franziska Emmerling [b], Dominik Al-Sabbagh [b], Juan Manuel García-Ruiz [a,*]

[a] Laboratorio de Estudios Cristalográficos, Instituto Andaluz de Ciencias de la Tierra (CSIC-UGR), Avenida de las Palmeras 4, Armilla, E-18100 Granada, Spain
[b] Federal Institute for Materials Research and Testing (BAM), Richard-Willstätter-Straße 11, 12489 Berlin, Germany

ARTICLE INFO

Editor: Christian France-Lanord

Keywords:
Crystallization sequence
Hydrochemical evolution
Alkaline brines
Soda lakes
Sodium carbonate minerals
Evaporite deposits

ABSTRACT

Soda lakes of the East African Rift Valley are hyperalkaline, hypersaline lakes extremely enriched in Na^+, K^+, Cl^-, CO_3^{2-}, HCO_3^-, and SiO_2. In this paper, we investigate the chemical evolution in these lakes and the production of chemical sediments by salt precipitation via evaporation. Water samples from tributary springs and three lakes (Magadi, Nasikie Engida and Natron) have been experimentally studied by in-situ X-ray diffraction during evaporation experiments to characterize the sequence of mineral precipitation. These data are complemented by ex-situ diffraction studies, chemical analyses and thermodynamic hydrochemical calculations producing detailed information on the activity of all solution species and the saturation state of all minerals potentially generated by the given composition. Major minerals precipitating from these samples are sodium carbonates/bicarbonates as well as halite. The CO_3/HCO_3 ratio, controlled by pH, is the main factor defining the Na-carbonates precipitation sequence: in lake brines where $CO_3/HCO_3 > 1$, trona precipitates first whereas in hot springs, where $CO_3/HCO_3 \ll 1$, nahcolite precipitates instead of trona, which forms later via partial dissolution of nahcolite. Precipitation of nahcolite is possible only at lower pH values (pCO_2 higher than -2.7) explaining the distribution of trona and nahcolite in current lakes and the stratigraphic sequences. Later, during evaporation, thermonatrite precipitates, normally at the same time as halite, at a very high pH (>11.2) after significant depletion of HCO_3^- due to trona precipitation. The precipitation of these soluble minerals increases the pH of the brine and is the main factor contributing to the hyperalkaline and hypersaline character of the lakes. Villiaumite, sylvite, alkaline earth carbonates, fluorapatite and silica are also predicted to precipitate, but most of them have not been observed in evaporation experiments, either because of the small amount of precipitates produced, kinetic effects delaying the nucleation of some phases, or by biologically induced effects in the lake chemistry that are not considered in our calculations. Even in these cases, the chemical composition in the corresponding ions allows for discussion on their accumulation and the eventual precipitation of these phases. The coupling of in-situ and ex-situ experiments and geochemical modelling is key to understanding the hydrogeochemical and hydroclimatic conditions of soda lakes, evaporite settings, and potentially soda oceans of early Earth and other extraterrestrial bodies.

1. Introduction

Soda lakes are saline lakes mostly found in endorheic basins dominated by volcanic terrains, like the tectonic depressions of the East African Rift valley. They are characterized by high pH and large concentration of Na^+, Cl^-, CO_3^{2-} and HCO_3^- (Deocampo and Renaut, 2016; Pecoraino et al., 2015; Schagerl and Renaut, 2016), leading to active evaporitic precipitation. Lake Magadi, Nasikie Engida (also known as Little Magadi), and Natron, hereafter MNN lakes, are among the highly saline and alkaline soda lakes in the East African Rift Valley where active precipitation of saline minerals and silica gels occurs (Fritz et al., 1987; Jones et al., 1977; Manega and Bieda, 1987). MNN lakes are located in the southern lowermost depression of the East African Rift valley, near the border between Kenya and Tanzania, occupying a N-S

* Corresponding author.
E-mail addresses: dessie.melese@csic.es (M. Getenet), otalora@iact.ugr-csic.es (F. Otálora), franziska.emmerling@bam.de (F. Emmerling), dominik.al-sabbagh@bam.de (D. Al-Sabbagh), juanmanuel.garcia@csic.es (J.M. García-Ruiz).

https://doi.org/10.1016/j.chemgeo.2022.121222
Received 9 June 2022; Received in revised form 31 October 2022; Accepted 15 November 2022
Available online 19 November 2022

trending axial graben. These basins are formed during the late-Pleistocene faulting of the metamorphic basements to the east and west (Baker, 1987; Baker et al., 1972; Dawson, 2008). The region passed through three stages of rifting namely pre-rifting regional doming, half-graben and full graben rifting which formed different basins filled with volcanic rocks of different composition, mainly alkali trachyte in the Magadi and Nasikie Engida region.

Three sedimentary units are defined in Magadi-Nasikie Engida region, from bottom to top, Oloronga Beds, Green Beds, and High Magadi Beds (Behr, 2002; Behr and Röhricht, 2000). The youngest sediments in the High Magadi Beds (named Evaporite Series) contain bedded trona intercalated with thin beds of tuffaceous clay and muds (Baker, 1958; Eugster, 1980, Eugster, 1967, 1967; Hay, 1968; Surdam and Eugster, 1976), and extend >65 m below Lake Magadi floor (Owen et al., 2019). During the Late Pleistocene to Holocene, the High Magadi Beds were deposited in a fresh to moderately saline, alkaline lake. Paleolake levels during the Early Holocene were high enough to allow the interconnection of Lake Magadi and Natron as a single water body (Baker, 1958; Eugster, 1980; Hillaire-Marcel et al., 1986). The modern evaporites of Natron consist of trona, nahcolite, thermonatrite and traces of halite and villiaumite interbedded with clays (Baker, 1986; Dawson, 2008; Manega and Bieda, 1987). Modern Lake Natron is surrounded by zeolitized clays and tuffs collectively called High Natron Beds (Baker, 1963; Hay, 1968); they contain irregular chert nodules with magadiite and kenyaite. The High Natron Beds may correlate with the High Magadi Beds, both deposited during the high stand periods that connected Lake Natron and Lake Magadi (Baker, 1963; Dawson, 2008; Hillaire-Marcel et al., 1986).

The dominant contributors to the solute content of the MNN brines are springs (Eugster, 1980; Jones et al., 1977; Renaut et al., 2020). Nasikie Engida hot springs emanate from a hot saline groundwater body (100–150 °C) recharged by the lower Ewaso Ngiro River and local groundwater (Allen et al., 1989). Apart from springs, Lake Natron is fed by four perennial rivers draining from the western escarpments and the highlands (Manega and Bieda, 1987). Dilute inflow reaches the lake through streams in the western rim of the rift valley and seasonal runoff from the north of Lake Magadi (Eugster, 1970; Jones et al., 1977). These inflows are rich in HCO_3^- and silica due to the rapid hydrolysis of volcanic rocks (Eugster, 1970; Jones et al., 1977), but poor in Al^{3+} due to precipitation of clays and gels (Eugster and Jones, 1968). Furthermore, before reaching the lake, dilute inflows and runoff waters undergo surface evaporation, producing efflorescent precipitation of alkaline earth carbonate crusts (Eugster, 1980), which reduce the concentration of Ca^{2+}, Mg^{2+} and HCO_3^- (Eugster, 1980; Eugster, 1970; Jones et al., 1977). During the next rainy season, the most soluble fraction of these crusts (halite and thermonatrite) is redissolved by rain and runoff water, increasing groundwater salinity, and leaving behind alkaline earth carbonates and silicates in the lake beds and alluvial flats. Recurrent precipitation and fractional dissolution of these crusts in a high geothermal gradient region give rise to saline groundwater that emerges in the form of warm and hot springs on the shore of Lake Magadi and northern Nasikie Engida, feeding it and evolving, mainly by evaporation, to brines rich in Na^+, Cl^-, CO_3^{2-}, and HCO_3^- that are saturated with respect to trona and/or nahcolite. Isotopic studies of evaporites of MNN lakes suggested an important contribution of Oldoinyo Lengai volcano to the salinity of these lakes (Bell et al., 1973). This volcano has been erupting natrocarbonatite lavas and ashes containing soluble sodium-potassium carbonate minerals (Dawson, 1964; Dawson, 1962), which are leached to give sodium-rich solution (Baker, 1986; Bell et al., 1973).

The brines of Lake Magadi and Nasikie Engida pass through a recurrent cycle of three stages: undersaturation, evaporative concentration, and desiccation. During evaporative concentration, trona grows as thin sheet-like rafts on the surface and as upward radiating needles at the bottom of the lake. After complete evaporation (desiccation stage), continued evaporation of interstitial brines causes expansion and buckling of the crust and precipitation of a variety of efflorescent crusts and intercrystalline cement. During the undersaturation stage (flooding of the lake), dilute inflows partially dissolve the pre-existing trona or nahcolite, depositing thin mud layers on top of the dissolution surfaces of previously deposited materials, i.e. layered upward radiating trona (in Lake Magadi) or nahcolite crystals (in Nasikie Engida) (Eugster, 1980; McNulty, 2017). In addition to trona/nahcolite, thermonatrite and halite precipitation occur at some local pools on the lake surface and in the evaporation ponds of TATA Chemicals Soda Company (Eugster, 1980; Renaut et al., 2020). Recently, McNulty (2017) presented a detailed discussion of the present sodium carbonate deposits of Lake Magadi and Nasikie Engida, comparing them with Late Pleistocene and Holocene lacustrine core sediments from Lake Magadi. A detailed discussion on the role of hydrothermal fluids in evaporite sedimentation at Nasikie Engida can be found in Renaut et al. (2020).

Many studies on saline lakes have shown the importance of understanding the mineral precipitation sequence to reveal the hydrochemical evolution of brines, and the paleoenvironmental conditions of ancient mineral deposits (Cabestrero and Sanz-Montero, 2018; Kolpakova and Gaskova, 2017; Lowenstein et al., 2016; Ma et al., 2011; Otálora et al., 2020; Renaut et al., 2020). The mechanisms of solute transport and the active precipitation of sodium carbonate minerals in soda lakes provide important insights into the depositional environment, paleo-brine chemistry, and diagenesis of evaporite deposits in the geological record. In this context, the assemblage of sodium carbonate minerals precipitated from brines can be used to constrain ancient temperatures and atmospheric CO_2 concentrations during deposition and, therefore in understanding the environmental and geochemical conditions of the past (Demicco and Lowenstein, 2019; Jagniecki et al., 2015; Olson and Lowenstein, 2021).

The extrapolation of the knowledge gained on the evaporite precipitation sequence from alkaline waters is also relevant for Precambrian studies and planetary sciences. Soda lakes have geochemistry close to that of the soda oceans in early Earth and other Earth-like planets and this geochemical context has been proposed for the origin of life on Earth (Kempe and Kazmierczak, 2002; Toner and Catling, 2020). Recently, we have demonstrated that self-assembled chemical gardens and vesicles can form from soda lake waters, suggesting the plausibility of their formation in the soda oceans of early Earth and other planets (Getenet et al., 2020). These mineral gardens and vesicles (specifically silica-based) have been shown to play an active catalytic role in the synthesis of prebiotically relevant compounds so they could have contributed to a planetary-scale transition from inorganic geochemistry to prebiotic organic chemistry (Bizzarri et al., 2018; García-Ruiz et al., 2020; García-Ruiz et al., 2017; Saladino et al., 2016).

Silica gels and chert deposits, like those in Lake Magadi and Nasikie Engida, are known to facilitate the accumulation and preservation of organic matter, so their study is expected to help in decoding the information on the early steps of life available within hydrothermal cherts of the Archean Earth (Behr, 2002; Behr and Röhricht, 2000; Eugster, 1967; Eugster and Jones, 1968; Hay, 1968; Reinhardt et al., 2019; Schubel and Simonson, 1990). This motivation for the study of Magadi deposits can be extended to planetary science. Sodium carbonate minerals characteristic of soda lakes have been reported to exist on extra-terrestrial planets. Lessons learned about the environmental constraints of these lakes can therefore be exported to the investigation of these planets (Carrozzo et al., 2018; De Sanctis et al., 2016; Glein et al., 2015; McCord et al., 1998). It has been also reported recently that phosphate accumulates in carbonate-rich soda lakes (Toner and Catling, 2020). The co-existence of high silica, carbonate, and phosphate content and the plausibility of mineral self-assembly in modern soda lakes implies that these lakes could be the “one-pot” geochemical environments containing all the important ingredients for the synthesis of prebiotically relevant molecules and plausible settings for the origin of life (García-Ruiz et al., 2020; Getenet et al., 2020).

Soda ash deposits are also economically important. They have been mined from active and ancient deposits from soda lakes (Schagerl and

Renaut, 2016; Smith and Carroll, 2015). At Lake Magadi, trona has been mined since 1911 to produce soda ash. Halite is also being produced in ponds where the brine has been evaporated beyond trona saturation (Schagerl and Renaut, 2016). Owing to their scientific and economic values, much work has been carried out on the mineral precipitation in soda lakes. Most of these studies are based either on field data or on thermodynamic modelling (Demicco and Lowenstein, 2019; Jagniecki and Lowenstein, 2015; Olson and Lowenstein, 2021; Renaut et al., 2020). Recent works have proven that a combination of field research, lab experiments and computer modelling is key to understanding evaporitic brine evolution and mineral precipitation sequences (Kotopoulou et al., 2019; Otálora et al., 2020; Rull et al., 2014). Recently, we have presented, and applied to Lake Magadi, a comprehensive methodology for monitoring evaporitic mineral precipitation and hydrochemical evolution of saline lakes (Getenet et al., 2022). Here, we expand this methodology and use it for the study of Lake Nasikie Engida and Lake Natron, discussing the geochemical and sedimentological perspective of evaporitic sediments in soda lakes based on experimental and geochemical modelling studies.

2. Methods and materials

2.1. Sampling and hydrochemical analysis

Lake brines and hot spring samples were collected from the three lakes during a field campaign in March 2018. The locations of the sampling are shown in Fig. 1. We have collected samples from both the hot spring and the lake brine of Nasikie Engida due to a significant spatial variation in hydrochemistry. The samples from the northern shore of Nasikie Engida were collected from one of the perennial hot springs that directly recharge the lake. During sampling, in-situ pH (±0.02), temperature (±0.15 °C), total dissolved solids (TDS; ±1 mg/L), electrical conductivity (EC; ±1 μS/cm), oxidation/reduction potential (ORP; ±1 mV), and saturation percent of dissolved oxygen (DO; ±1%) were recorded by using Hanna HI 9829 multiparametric probe.

CO_3^{2-} and HCO_3^- concentrations were determined by potentiometric titration at the Laboratorio de Estudios Cristalográficos (LEC) of the Instituto Andaluz de Ciencias de la Tierra (IACT) in Granada (Spain) and ALS Laboratory Group (Czech Republic). Cl^-, F^- and SO_4^{2-} were analyzed using ion liquid chromatography and ion selective electrode at ALS and Instituto de Catálisis y Petroleoquímica-CSIC (Spain). SiO_2 was analyzed by using inductively coupled plasma optical emission spectrometry and discrete spectrophotometry at the Technical Services of the Estación Experimental del Zaidín-CSIC (Spain) and ALS. All the remaining chemical analyses were performed by ALS laboratory: Na^+, K^+, Mg^{2+}, Ca^{2+}, Al^{3+}, Fe (total), B^+, and Br^- were determined using inductively coupled plasma mass spectrometry (ICP-MS). The samples were fixed by the addition of nitric acid prior to analysis with ICP-MS. PO_4^{3-} was determined by a colorimetric method based on molybdenum blue using discrete spectrophotometry.

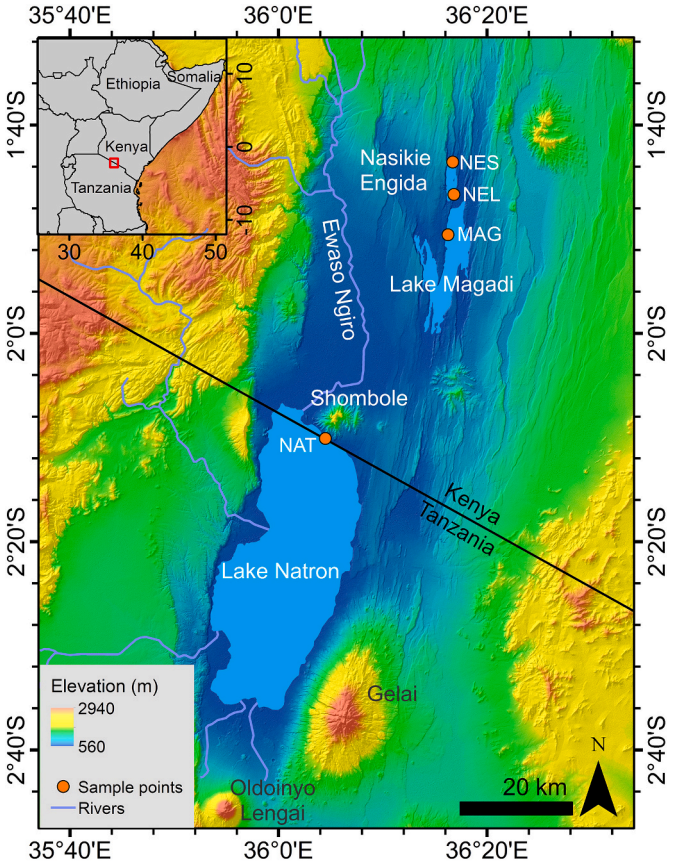

Fig. 1. Digital elevation model map of the MNN basin, the sampling points (NES: Nasikie Engida hot spring (1° 43.56′ S, 36° 16.71′ E), NEL: Lake Nasikie Engida brine (1° 46.67′ S, 36° 16.82′ E), MAG: Lake Magadi brine (1° 50.54 S, 36° 16.25′ E), NAT: Lake Natron brine (2° 10.1′ S, 36° 4.49′ E)), and the volcanos in its vicinity. Digital elevation data © NASA Shuttle Radar Topography Mission.

2.2. Evaporation experiments and ex-situ characterization of precipitates

Ex-situ evaporation and mineral precipitation experiments were performed at 30 ± 1 °C on glass slides except for Lake Magadi brine which are performed at 25 ± 1 °C. Relative humidity was maintained at 35 ± 2% by using a climate chamber (Memmert, Germany). Droplets of about 25 μL (approximate diameter 1 cm) were poured on glass slides using plastic pipettes. After complete evaporation of the droplets, the mineralogy of the precipitates was characterized by using powder X-ray diffraction. For ex-situ X-ray diffraction, we used a high-resolution Bruker D8 Advance X-ray diffractometer (at the Laboratorio de Estudios Cristalográficos) with monochromatic Cu $K_{\alpha 1}$ radiation, primary Ge (111) monochromator and a Lynxeye PSD detector). Diffractograms were acquired in transmission mode, at 40 kV acceleration voltage, and 40 mA current, 2θ scans spanning from 5° to 80° with a 2θ step of 0.02° per second. Malvern Panalytical HighScore software (version 4.9) with the ICCD PDF-4+ (2020) database was used for phase identification.

2.3. In-situ characterization of precipitates

Transformation between different hydrates of sodium carbonate-bicarbonate minerals, along with secondary precipitation, can happen even during sample handling for ex-situ characterization, which will challenge the accurate determination of the precipitation sequence. To overcome these problems, we have performed in-situ X-ray diffractions of containerless levitated droplets.

In situ X-ray diffraction data was collected from evaporating levitated droplets to track the time evolution of mineral precipitation during evaporation. These experiments were performed at the μSpot beamline (see Paris et al., 2007 for detail) at the BESSY II synchrotron (Helmholtz Centre Berlin for Materials and Energy, Berlin, Germany), using the protocol described in Wolf et al. (2008). The beamline features an acoustic levitator used as a containerless sample holder (see the experimental setup in Getenet et al. (2022). In a typical experiment, 5 μL of the sample were pipetted in one of the nodes of the standing acoustic wave of the levitator to form a drop with an approximate diameter of 2 mm. A 0.72929 Å wavelength, 100 μm size incident beam was used. Scattered intensities were collected by a two-dimensional detector (Eiger9M, CCD 3072 × 3072). The exposure time was 5 s. Evaporation was followed for 30–80 min until complete desiccation. The obtained diffraction images were processed in DPDAK (Benecke et al., 2014) and converted to scattering vector q. The scattering vector was converted to

the interplanar distance d by using pre-processing Python script. The evolution of the size of the levitated droplet during evaporation was monitored with a video camera. Levitated drop evaporation was performed at 30 ± 1 °C except for the Lake Magadi sample which was evaporated at 25 ± 1 °C and relative humidity of 35 ± 2%. The pCO_2 of both the in-situ and ex-situ experimental conditions were not constrained, so we assumed that the experimental pCO_2 is equivalent to atmospheric pCO_2 (−3.4).

2.4. Computer modelling

We used the PHREEQC version 3.4 code and an updated Pitzer database for thermodynamic hydrochemical speciation, evaporation and precipitation calculations (Parkhurst and Appelo, 2013). The standard PHREEQC pitzer.dat database was updated with data for fluorite, hydroxyapatite, and fluorapatite taken from the llnl.dat database (Parkhurst and Appelo, 2013) and chlorapatite from Thermoddem database (v1.10) (Blanc et al., 2012). For villiaumite (NaF), thermodynamic data were taken from ThermoChimie database (v10a) (Giffaut et al., 2014). Parameters for thermonatrite, $Na(H_2PO_4)$ and its hydrated forms were taken from Toner and Catling (2020). Evaporation was simulated at 30 °C. In the case of Lake Magadi, simulations were performed at 25 °C (the temperature at which experiments of this specific sample performed) and 30 °C to compare with the rest of the lakes. All our PHREEQC calculations started with the actual brine composition measured in samples from the lakes. During simulation, we assumed no equilibrium with the atmosphere because CO_2 dissolution into the quickly evaporating droplets is not significant compared with the pCO_2 changes induced by mineral precipitation/dissolution.

3. Results

3.1. Hydrochemistry

Table 1 shows the in-situ and laboratory measurements of the hydrochemical parameters of the MNN brines used for the evaporation experiments. Fig. 2 shows the relative composition of major anions (CO_3^{2-}, HCO_3^- and Cl^-), the concentration of Na^+ and the pH of the four samples. The pH was very alkaline, varying between 9.1 (in the Nasikie Engida hot spring) and 10 (in Lake Natron). These samples are considerably rich in SO_4^{2-}, F^-, SiO_2, PO_4^{3-} and Br^-. However, they are highly depleted in Ca^{2+}, Mg^{2+}, Al^{3+}, B^+ and Fe.

Lake Nasikie Engida brine has the highest concentration of major ions. It is evident from the total dissolved solids and the ionic strength that Lake Nasikie Engida brines are relatively the most enriched in solute contents (Table 1). Lake Nasikie Engida brines are mainly recharged by hot springs on its northern shoreline. Hence, the lake brine is the result of the hydrochemical evolution of the hot springs waters, which give rise to the significant enrichment in major ions except for HCO_3^- (Fig. 2). Despite this fact, Lake Nasikie Engida brine contains nearly equivalent amounts of HCO_3^- ions as the hot spring in absolute terms. Lake Natron brine contains the second highest concentration of Na^+, Cl^-, CO_3^{2-}, K^+ and SO_4^{2-} whereas its HCO_3^- and SiO_2 content was the lowest (Fig. 2 and Table 1). The hot spring contains the highest HCO_3^- because of its lower pH and shows the lowest K^+, F^- and CO_3^{2-} concentrations (see Fig. 2 and Table 1). Lake Magadi brine contains an intermediate concentration of solutes among the three lakes while its Cl^- and SO_4^{2-} ions are relatively the lowest among all samples.

3.2. Ex-situ powder X-ray diffraction

Powder X-ray diffraction of the whole precipitates obtained from the evaporation of droplets revealed the presence of trona, thermonatrite, halite, and sylvite in all samples studied (Fig. 3a-d). In addition to these phases, nahcolite was detected in Nasikie Engida hot spring (see Fig. 3c). The diffraction peaks of nahcolite are broad whereas that of trona are weak relative to the diffraction patterns from lake brines (Fig. 3c), most likely due to a phase transition from trona to nahcolite.

Table 1
Results of the in-situ brine characterization and the laboratory chemical analysis of samples used for the evaporation and precipitation experiments. Ionic concentrations are in ppm.

	Lake Magadi	Nasikie Engida	Nasikie Engida	Lake Natron
Sample type	lake	lake	hot spring	lake
Sample label[a]	MAG	NEL	NES	NAT
In-situ pH	9.8	9.7	9.1	10
Temperature (°C)	29.2	24.7	79.4	40.1
EC (mS/cm)	68.6	104.8	39.04	43.05
TDS (g/L)	38.1	52.42	19.51	21.52
ORP (mV)	−464.7	18	−36.6	−39.6
DO (%)	46.2	72	127.2	143.2
Ionic strength (M)	0.74	2.65	0.64	0.79
Na^+	12,850 ± 1285	43,300 ± 4330	12,700 ± 1270	13,000 ± 1300
K^+	228.5 ± 23	1145 ± 115	196 ± 20	364 ± 36
Cl^-	5250 ± 788	37,600 ± 5640	6060 ± 909	8700 ± 1305
CO_3^{2-}	9600	30,500 ± 3660	3910 ± 469	9710 ± 1165
HCO_3^-	6100	15,200 ± 1824	15,700 ± 1884	5340 ± 641
SO_4^{2-}	100.5 ± 15	451 ± 67.6	334 ± 50	375 ± 56.3
SiO_2	91.4	193 ± 38.6	65.8 ± 13.2	51.2 ± 10.2
F^-	208 ± 31	434.6	120.5	163.2
PO_4^{3-}	19.4 ± 3.9	26.5 ± 5.3		40.1 ± 8
Mg^{2+}	12 ± 0.12	1.25 ± 0.13	0.072 ± 0.0072	3.02 ± 0.3
Ca^{2+}	4.5 ± 0.45	5.1 ± 0.51	0.501 ± 0.05	19 ± 1.9
Al^{3+}	<0.05	0.62 ± 0.062	<0.02	8.5 ± 0.85
Fe^{tot}	0.1 ± 0.01	0.16 ± 0.016	0.05 ± 0.005	7.3 ± 0.73
B^+	5.2 ± 0.52		9.5 ± 0.95	
Br^-	23.3 ± 2.3		30.2 ± 3	

[a] Sample label refers to the labels of the sampling points in Fig. 1.

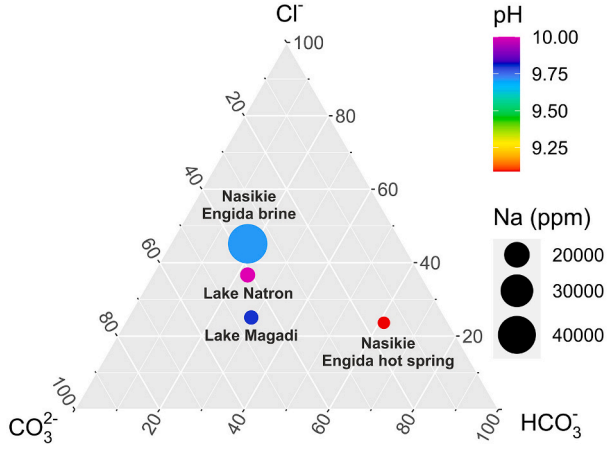

Fig. 2. Composition of the four samples shown in Table 1. Point positions in the triangular plot correspond to the relative anionic composition. The size of the points corresponds to the concentration of Na (roughly proportional to TDS). The colour of the points corresponds to the in-situ measured pH at sampling time.

3.3. In-situ evaporation of levitated droplets

Fig. 4a-d shows the in-situ X-ray diffraction measurements collected

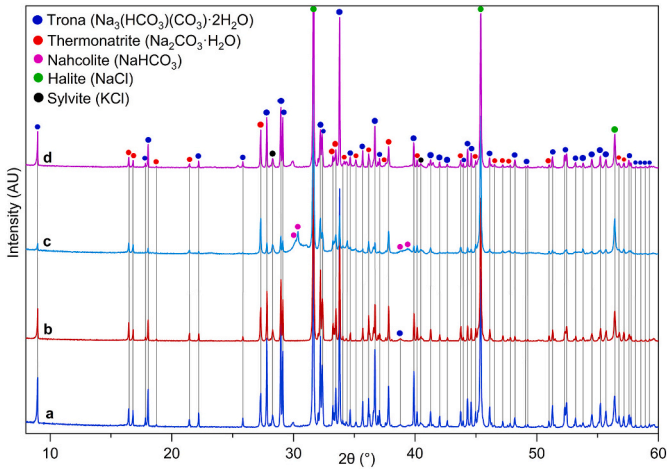

Fig. 3. Powder X-ray diffraction of the whole precipitates obtained by evaporation of (a) Lake Magadi brine, (b) Lake Nasikie Engida brine, (c) Nasikie Engida hot spring and (d) Lake Natron brine.

during evaporation of acoustically levitated droplets of MNN lakes and hot spring brines. Trona precipitates first after 2670, 1595, and 1725 s of evaporation of Magadi, Nasikie Engida and Natron lake brines respectively (see Fig. 4a-b,d; the blue bars). In Nasikie Engida hot spring, nahcolite and amorphous silica simultaneously appear first after 1630 s of evaporation (Fig. 4c; magenta bars). Unidentified phase with a single diffraction peak appeared with nahcolite and amorphous silica in Nasikie Engida hot spring (? in Fig. 3c). Halite was the second phase to appear in all samples. Precipitation of halite began after 2855, 1645, 1805 and 1790 s in Magadi, Nasikie Engida lake and hot spring and Natron respectively (see Fig. 4a-d; the green bars). Thermonatrite appeared in a third place after 2955, 1950 and 1970 s in Magadi, Nasikie Engida hot spring and Natron respectively (Fig. 4a,c,d; the red bars). Finally, precipitation of sylvite starts after 1990 and 2100 s in Nasikie Engida hot spring and Lake Natron respectively (Fig. 4c-d; grey bars). The phases observed in in-situ evaporation are in good agreement with the ex-situ experiments except for a few discrepancies: sylvite and/or thermonatrite didn't appear in the in-situ evaporation of Lake Magadi and Nasikie Engida brines while these phases were detected in ex-situ experiments (Fig. 3a-b). Trona, which was not detected during in-situ evaporation of Nasikie Engida hot spring bine, was observed in ex-situ evaporation (Fig. 3c). These differences are most likely related to the smaller volume of the levitated drops and the resulting smaller volume of precipitated minerals. In the case of Nasikie Engida hot spring, trona observed in the ex-situ diffraction could be the result of partial transformation of nahcolite during sample handling (Fig. 3c), which would not happen in the real-time diffraction measurements.

3.4. Thermodynamic modelling of evaporation

Thermodynamic models are valuable not only for predicting the phase assemblages and the relative amount of the phases precipitated but also for the resulting hydrochemical evolution during evaporitic mineral precipitation. To test our experimental results, we performed a set of geochemical modelling simulations using the PHREEQC code. Evaporation and mineral precipitation were simulated by computing successive equilibrium states separated by discrete, small removals of water from the solution. Fig. 5 shows the output of these models in terms of the precipitation sequence of different minerals (left), and ionic concentration (right) versus concentration factor (CF; the ratio between the initial brine volume and the "current" volume at this point). The output of the model reproduces very well the experimental observations of major phases precipitation.

3.4.1. Sodium carbonates

The precipitation sequence of sodium carbonate phases shows two clearly distinct trends. In the sample from the Nasikie Engida hot spring, nahcolite is the first phase to precipitate (CF = 3.4) and the dominant one during the evaporation process (Fig. 5e). Precipitation of nahcolite stops after reaching a peak amount of 0.2 mol/kg at a CF = 14, but the dissolution of nahcolite after this point is small and this phase stays stable upon subsequent evaporation. Nahcolite and trona are the only sodium carbonate phases precipitating during evaporation of Nasikie Engida hot spring waters. In contrast, the three samples from the different lakes produce, during evaporation, first a short, transient period of nahcolite precipitation starting at CFs of 6 (Lake Magadi), 1.9 (Nasikie Engida) and 7.2 (Lake Natron) (Fig. 5a,c,g). Shortly after this event, trona starts to precipitate at CFs of 9.7 (Lake Magadi), 2.2 (Nasikie Engida) and 8.2 (Lake Natron), which ends the precipitation of nahcolite and initiates its dissolution, causing the quick disappearance of this phase. At CFs of 62.6 (Lake Magadi), 8.8 (Nasikie Engida) and 27.6 (Lake Natron), thermonatrite starts precipitating. Trona precipitation is already negligible at this stage during evaporation; after reaching CFs of 30 (Lake Magadi), 5 (Nasikie Engida), and 20 (Lake Natron), trona no longer precipitates leaving a constant amount of trona. The brine from Lake Nasikie Engida shows a sudden transformation of thermonatrite into natron at a CF of 17.8.

In summary, after complete evaporation, the hot spring sample produces a mix of nahcolite (roughly 65%) and trona (roughly 35%), while samples from lake waters produce a mix of trona and thermonatrite (in Lake Magadi and Lake Natron) or trona and natron (in Lake Nasikie Engida). Trona is always dominant in the lake samples with ratios depending on the initial chemistry.

The ionic concentration follows the precipitation of the different phases. All ions increase linearly (in a logarithmic scale) with the concentration factor until a phase that contains that ion starts precipitating (Fig. 5b,d,f,h). pH initially decreases linearly with evaporation until sodium carbonate phases start precipitating. From this point on, pH is controlled by the precipitation of these phases. CO_3^{2-} is the dominant C species in lake brines during evaporation while HCO_3^- is dominant at the beginning in the hot spring sample. The precipitation of nahcolite and trona depletes the concentration of HCO_3^- and increases the pH of the brine. The subsequent reduction of HCO_3^- concentration slows down the precipitation of trona and eventually undersaturate the brine with respect to nahcolite that starts dissolving. At higher pH values and with slow precipitation of trona, other carbonates, specially thermonatrite, start precipitating except in the case of the hot spring, where the HCO_3^- concentration is higher (although CO_3^{2-} is dominant for CFs higher than 9). This, along with the lower pH, hinders the precipitation of thermonatrite (Fig. 5e-f). In all cases, Na^+ is, by far, the dominant cation during the whole evaporation/precipitation process although its concentration is reduced significantly by the end of the evaporation due to the precipitation of sodium carbonate minerals and halite.

3.4.2. Halides

Halite is the main chloride predicted to precipitate, and the only one in samples from Lake Natron and Nasikie Engida hot spring. Precipitation of halite starts at CFs of 31 (Lake Magadi), 4.5 (Nasikie Engida lake), 33.2 (Nasikie Engida hot spring) and 19.3 (Lake Natron) and lasts till the end of the evaporation (Fig. 5a,c,e,g). The highest predicted amount of halite (895 mmol/kg) was obtained from Lake Nasikie Engida brine. In Lake Magadi and Nasikie Engida brines, sylvite starts precipitating at CF of 300 (Lake Magadi) and 27.3 (Lake Nasikie Engida), reaching a maximum amount of roughly 3% of halite.

Villiaumite is the only fluoride predicted to precipitate from these brines with high F^-, but low Ca^{2+}. Precipitation starts at a CF = 30 (Lake Magadi), 10.3 (Nasikie Engida lake), 47.6 (Nasikie Engida hot spring) and 32.6 (Lake Natron). The concentration of F^- increases linearly until villiaumite starts precipitating and then stays almost constant at around 0.25 *m* (Fig. 5b,d,f,h).

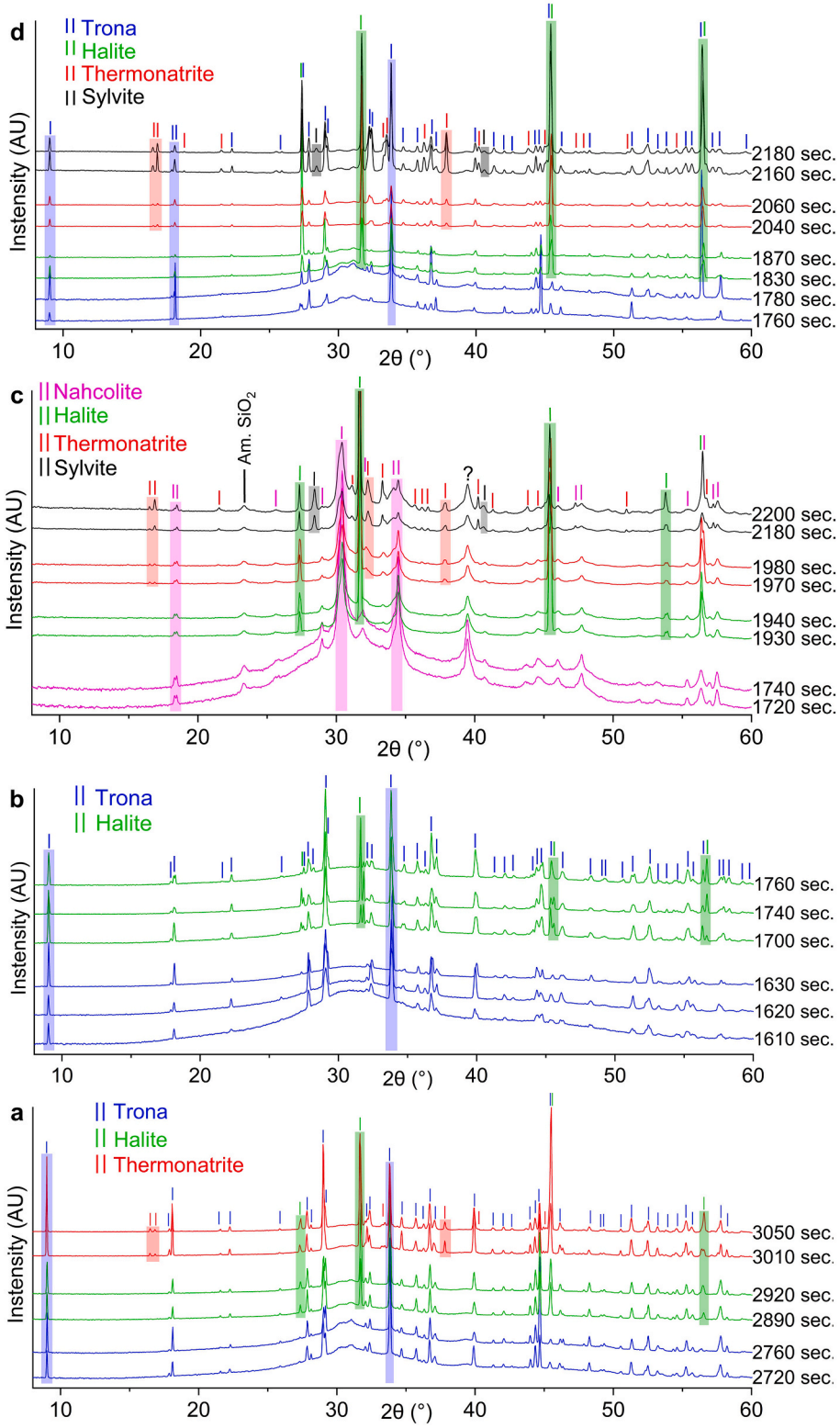

Fig. 4. X-ray diffractograms collected during the evaporation of levitated droplets of (a) Lake Magadi brine (modified from Getenet et al. (2022)), (b) Lake Nasikie Engida brine, (c) Nasikie Engida hot spring and (d) Lake Natron brine. Note that the first diffractograms of the corresponding colour are taken a few seconds after the characteristic peaks of the given phase are clearly visible. The exact time when each mineral starts to precipitate is reported in the text.

3.4.3. Silica

Silica precipitation also shows a clearly different trend in lakes and hot spring waters. In lake samples, there are two silica precipitation periods during evaporation, one at the beginning, CF value 3–17 (Lake Magadi), 1–8 (Nasikie Engida) and 1–20 (Lake Natron), and the other to the end, close to complete evaporation, after CF = 275 (Lake Magadi), 11.6 (Lake Nasikie Engida) and 60 (Lake Natron). In between, there is a period of silica dissolution related to a sudden increase in pH during evaporation (Fig. 5a,c,g). In contrast, silica precipitates continuously during all the evaporation of the hot spring brine (Fig. 5e). Silica species

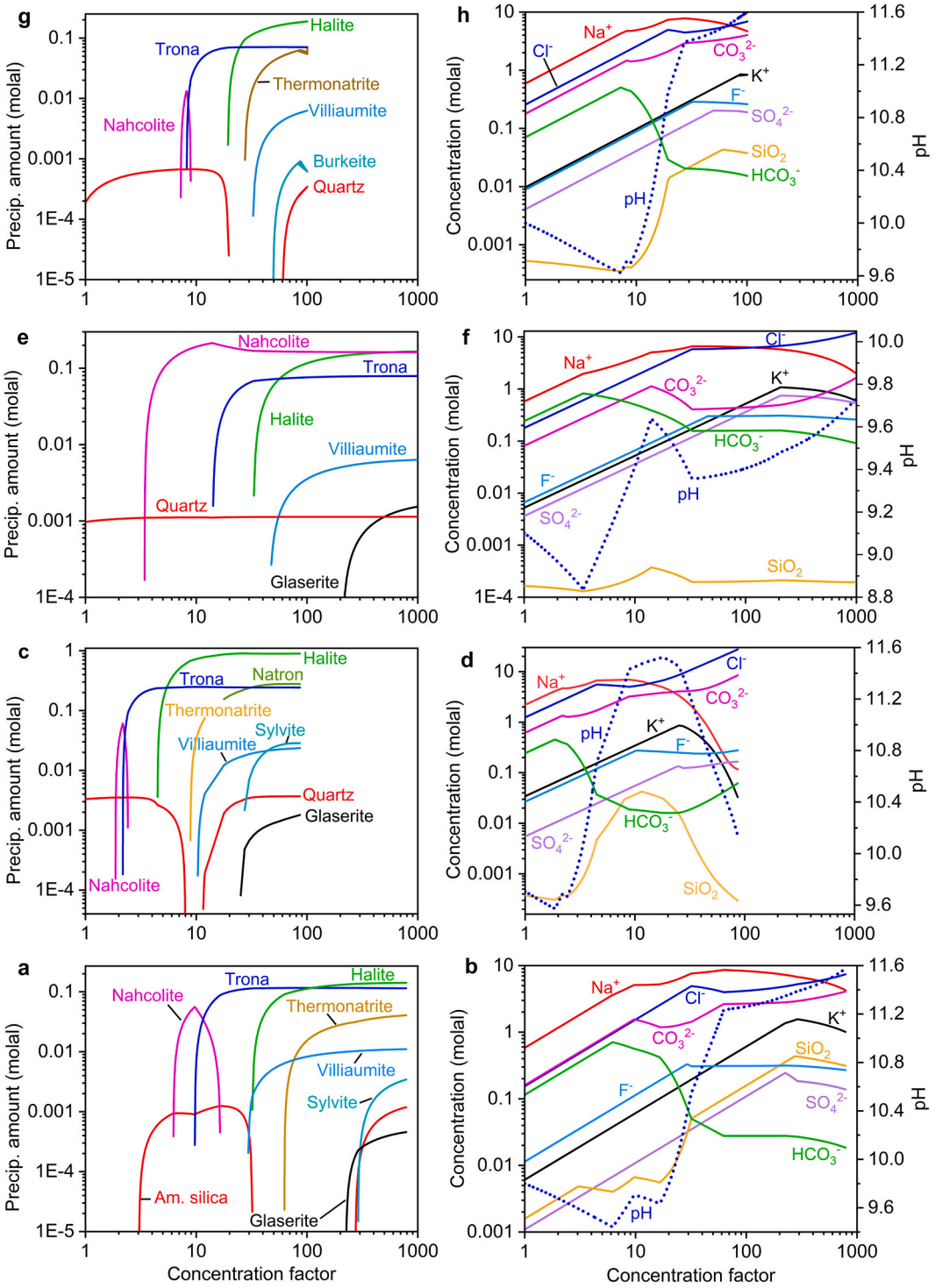

Fig. 5. PHREEQC simulation of evaporation and mineral precipitation from Lake Magadi brine at 25 °C (a–b), Lake Nasikie Engida brine (c–d), Nasikie Engida hot spring (e–f), and Lake Natron brine (g–h) at 30 °C: the mineral precipitation sequence and the amount of precipitates (left panels) and hydrochemical evolution of the brines during mineral precipitation (right panels). Note: the simulation of Lake Magadi brine at 30 °C gave similar results to panels a and b except for quartz precipitation instead of amorphous silica (see Fig. S1). The maximum CFs vary across samples depending on the point of divergence of the numerical equations during simulation.

in solution closely follow the evolution of pH, controlled by the precipitation of sodium carbonate minerals, increasing when pH increases and decreasing elsewhere because higher pH values increase the solubility of SiO_2 (Krauskopf and Bird, 1979). The dependency on pH is even higher than the dependency on evaporation. The type of precipitating silica phases is controlled by temperature. At 25 °C, Lake Magadi brine reached supersaturation with respect to amorphous silica (Fig. 5a) whereas at a relatively higher temperature (30 °C), evaporation may led to quartz precipitation (see Fig. 5c,e,g and Fig. S1).

3.4.4. *Other minerals*

Owing to the low sulphate and calcium content of the brines,

sulphate precipitation is scarce and restricted to very small amounts of glaserite ($(Na,K)_3Na(SO_4)_2$) and burkeite ($Na_6(CO_3)(SO_4)_2$). The second is predicted to precipitate only in samples from Lake Natron at high CF values (higher than 50) (Fig. 5g) while glaserite is expected to precipitate from the remaining brines at CF of 205 (Lake Magadi), 25.2 (Lake Nasikie Engida) and 220 (Nasikie Engida hot spring) (Fig. 5a,c,e). The final amount of these precipitates goes from 0.5 to 3 mmol/kg.

The initial lake brines were supersaturated with respect to fluorapatite, magnesite, and talc (see Fig. S1,S3,S5,S7,S8). In the absence of phosphate ions, the lake brines were initially supersaturated with calcite instead of fluorapatite (Fig. S3,S5,S8). Nasikie Engida hot spring brine was initially supersaturated with respect to calcite, followed by subsequent precipitation of a minor amount of dolomite, pirssonite, fluorite and borax after a CF of 1.4 (Fig. S6a). Fluorapatite and pirssonite precipitation is coupled due to the competition for Ca^{2+}, the precipitation of one of them being triggered by the dissolution of the other (Fig. S4a, S7a). Gaylussite is also predicted to precipitate as evaporation of Lake Magadi and Nasikie Engida waters advance (Fig. S3, S5). Neither of these phases was observed in the experimental results possibly due to their minor contribution (<1 mmol/kg) or the absence of Ca-bearing particles and inflows that upon interaction with alkaline brines would form, for example, gaylussite. The precipitation of these phases kept Ca^{2+} and Mg^{2+} species below 20 μmol/kg (Fig. S1-S8b). Phosphate, boron, and bromine rise linearly with evaporation (Fig. S1-S8b). Boron concentration rises with evaporation until a CF of 306 in Nasikie Engida hot spring and then is predicted to precipitate as borax, depleting the boron concentration (Fig. S6).

4. Discussion

4.1. Major phases

The observed and simulated mineral precipitation sequences reflect the integrated effects of temperature, brine composition, and pCO_2. The combination of temperature and pCO_2 control the stability of different Na-carbonate phases (Eugster, 1966; Jagniecki et al., 2015). In turn, the initial pCO_2 was imposed by the measured composition of the brines. The relative composition of ionic species in the initial brines determine the resulting mineral assemblages, the precipitation sequence, and their relative abundance. The main variability found in our study corresponds to the different precipitation sequences from lake brines and hot springs, the latter having a lower pH and CO_3/HCO_3 concentration ratio. From lake brines, the precipitation sequence trona > halite > thermonatrite is consistently predicted and observed (both in-situ and ex-situ). The brine from Lake Nasikie Engida also follows this sequence, but thermonatrite is only observed in the ex-situ experiments. Furthermore, the transformation of thermonatrite into natron is predicted by simulation, but natron was not observed in the experiments. The sequence for the hot-spring brine is clearly different. Its starts with the precipitation of nahcolite, which is the dominant phase during the whole evaporation process. Next, a smaller amount of trona is predicted to precipitate, and was observed in the ex-situ experiments, but not in the in-situ ones. Halite is the next phase predicted and observed. No further Na-carbonate phases are predicted to precipitate, but a small amount of thermonatrite was detected in both the in-situ and ex-situ diffraction experiments. This discrepancy could be due to a kinetic effect; the equilibrium calculation predicts the precipitation of trona after nahcolite, but in the relatively fast evaporation experiments we may reach the precipitation of halite before trona actually precipitates even if the brine is supersaturated with respect to trona. This lack of trona precipitation drives out the fast decrease in pH at CF = 11, which finally produces the precipitation of thermonatrite. A similar effect of delayed nucleation is most likely the reason for not observing neither thermonatrite in the in-situ experiments of Lake Nasikie Engida nor the short, transient nahcolite precipitation at the beginning of evaporation.

Full evaporation sequences are not expected to be observed in the lakes, but only in efflorescent crusts. The composition of lake brines reflects the seasonal evolution of incoming waters upon recurring hydrologic cycles and the seasonal variation of outcoming water by evaporation. During rainy seasons, the water inflow increases and evaporation decreases, driving the brine composition closer to the hot-spring waters. The reverse process happens during dry seasons. Mixed saline and freshwater diatoms, dissolution surfaces and muddy layers found in the evaporite sequences of Lake Magadi evidence seasonal/periodic flooding of the paleolake brine with dilute water (Buatois et al., 2020; Owen et al., 2019), which happens in the modern deposits (McNulty, 2017; Owen et al., 2019; Renaut et al., 2020). Depending on the amplitude and duration of these periods as well as on the lake volume, the resulting evaporitic sequence can show different combinations of sodium carbonate minerals, although the careful study is required for this because nahcolite may also form during diagenesis through bacterial CO_2 addition to the interstitial brines (Eugster, 1980). Lowenstein et al. (2017) suggested CO_2 input from the decay of organic matter in Green River lakes (USA), leading to precipitation of trona and nahcolite.

Lake Magadi, the southern section of Nasikie Engida and Natron are covered by mainly trona crust and efflorescent thermonatrite and halite (Dawson, 2008; Renaut et al., 2020), which corresponds to the "lake precipitation sequence". Trona has been forming for the last hundred thousand years, forming a 65 m sequence in Lake Magadi (Owen et al., 2019), but drill cores on Lake Magadi (uppermost 65 m of the core) contain nahcolite as well (Baker, 1958; Owen et al., 2019), indicating periods of higher spring inflow in the past.

Nahcolite was observed in southern Nasikie Engida, but it is dominantly forming in the northern part of the lake where perennial saline hot springs fed the lake and where magmatic CO_2 emanate via deep faults (Lee et al., 2017; Lee et al., 2016; Renaut et al., 2020). The evaporite sediments of northern Nasikie Engida are dominated by nahcolite (De Cort et al., 2019; Renaut et al., 2020). Nahcolite was more widespread in the past. Drill cores on the lakebed revealed that the uppermost 374 cm sediments are composed of intercalations of laminated mud with scattered nahcolite crystals and distinct beds of nahcolite resulting from abrupt precipitation at the sediment-water interface or within the water column (De Cort et al., 2019). Towards the centre of the southern Nasikie Engida, layers of up to 3 cm long nahcolite crystals were found beneath the trona beds (Renaut et al., 2020), indicating periods of higher HCO_3 concentration in the past. Hot spring brines are mostly contributed to the lake, but part of them end up gathered around hot spring vents and their outflow channel. There a full evaporation sequence from nahcolite to thermonatrite is expected. Renaut et al. (2020) reported efflorescent crusts of trona, nahcolite, thermonatrite and halite around spring vents on the northern shore of Nasikie Engida.

In Lake Natron we found the opposite situation, with no nahcolite in the evaporitic record. Here trona was reported both in ancient and modern evaporite deposits. The modern surface of Lake Natron is composed of 10–20 cm thick trona, thermonatrite and halite crust (Fritz et al., 1987; Manega and Bieda, 1987). Sediments collected on the lake bottom have shown alternating layers of black clay and trona (Hay, 1966). Trona moulds and casts were found in a horizon of mid-Pleistocene lacustrine sediments of Peninj beds on the west side of Lake Natron. These beds were deposited in a highly saline sodium-carbonate rich lake, which was analogous to the modern Lake Natron (Hay, 1968; Hay, 1966; Isaac, 1967; Isaac, 1965). These differences are most likely due to the much larger water volume, which makes larger the volumetric ratio between evolved lake brines and the relatively fresh spring brines.

Thermonatrite and halite form only in the modern evaporite sequence of MNN lakes as efflorescent crusts and some local pools where there is intense evaporation (Eugster, 1980; Renaut et al., 2020). These minerals were not reported in the ancient deposits due to either the paleolake brines did not reach supersaturation or they precipitated but re-dissolved during an episodic freshening of the paleolake brines. In

contrast to the natural lakes, a significant amount of thermonatrite and halite precipitate respectively at the bottom and on the surface of the artificial pans of TATA chemicals company, made for the commercial production of salt by harvesting the top layer of halite (Eugster, 1980; Eugster, 1971). This fact is explained by our results: the company pumps the HCO_3-depleted lake brine (after trona precipitation) into shallow evaporation ponds where evaporation is very rapid and organic production of CO_2 is negligible. Fast evaporation in these ponds, as in our experiments, precipitate a large amount of thermonatrite and halite with some trona (Eugster, 1980, Eugster, 1971).

In the natural settings, trona and nahcolite precipitate as thick layers whereas thermonatrite and halite were minor components. However, our experimental observations show that a considerable amount of thermonatrite and halite form in addition to trona. Moreover, the predicted final amount of halite was greater than that of trona and nahcolite in all cases (Fig. 5 a,c,g). The difference in the relative amount of the minerals among the experiments and models and the natural setting arises from the difference in partial CO_2 pressure (pCO_2). It has been shown that excess CO_2 input is a crucial pre-condition for the formation of thick deposits of trona and nahcolite to replenish the depleting HCO_3^- and CO_3^{2-} ions (Bradley and Eugster, 1969; Earman et al., 2005; Eugster, 1980; Eugster, 1966; Jagniecki et al., 2015; Lowenstein and Demicco, 2006). Nahcolite, trona and thermonatrite precipitates to an amount lower than that of halite in the simulations due to the lower CO_3^{2-} or HCO_3^- compared to Cl^- and the fast evaporation leading to a limited amount of atmospheric CO_2 dissolved into the brines. Trona deposits with minor thermonatrite could have been possible in Lake Magadi and Natron due to biogenic CO_2 input; if this additional CO_2 were not available, a significant amount of thermonatrite would have formed in addition to trona. At least between 10 and 80 °C, the pCO_2 level required for nahcolite stability is higher than that required for trona precipitation, which could happen under current atmospheric conditions ($pCO_2 \approx -3.4$) (Bradley and Eugster, 1969; Eugster, 1980; Eugster, 1966; Jagniecki et al., 2015; Lowenstein and Demicco, 2006). Our simulations show that precipitation and stability of nahcolite is possible only at $pCO_2 > -2.7$. In lake brines, the pCO_2 was higher than -2.7 only until the onset of nahcolite precipitation. Hence, the early precipitated nahcolite dissolves almost completely (Fig. 5 a,c,g). Only the hot spring was able to form a detectable amount of nahcolite after complete evaporation (Fig. 3c, Fig. 4c). The transformation from nahcolite to trona seems evident from the poor crystallinity of nahcolite and the weak peaks of trona in ex-situ diffractions (see Fig. 3c). Natron was predicted to form in southern Nasikie Engida brine (Fig. 5c) but was not observed in our experiments nor reported in Nasikie Engida studies. Eugster (1980) observed natron crystallization in Lake Magadi during cool nights which convert to trona in the morning when the temperature increase. Natron precipitation is not expected in East African Soda Lakes because it's a low temperature phase of Na-carbonates (Eugster, 1966; Jagniecki et al., 2015). In East African Soda Lakes, natron would have precipitated below 32 °C but this needs to be combined with pCO_2 significantly lower than the atmospheric one (see the stability fields in Eugster (1966) and Jagniecki et al. (2015)), which is not possible owing to the equilibration of lake brines with the atmosphere.

Our results show a lower variety of precipitated phases in the X-ray diffraction experiments than in the simulations. This fact is clearly due to the diffraction detection limit. In addition to sodium carbonate phases and halite, the next more abundant mineral predicted by simulations is villiaumite, with amounts in the range of 6–20 mmol/kg of brine. Since the typical volumes of droplets are 25 μL for ex-situ experiments and 5 μL for the in-situ ones, the maximum expected amount of villiaumite would be around 0.021 μg for the ex-situ experiments and 0.0042 μg for the in-situ ones. These small amounts explain the lack of detection of minerals predicted to precipitate at levels close to or below 20 mmol/kg.

4.2. Phosphates and fluorides

Phosphate accumulates in soda lakes due to calcium sequestration by carbonate minerals precipitation, which results in a lack of apatite precipitation (Toner and Catling, 2020). This accumulation can reach levels relevant to the synthesis of prebiotic biomolecules. MNN samples were supersaturated with respect to fluorapatite since the beginning of evaporation. The amount of fluorapatite eventually precipitated is limited to very low amounts by the extremely low calcium content so this phase has not been reported in these lakes. As a result, phosphate concentration increases linearly with evaporation (Fig. S2, S4, S7). Thermodynamic simulations, which don't include biological processes, seem to overestimate the actual phosphate concentration, which is actually lower after microbial phosphate consumption and deposition with organic matter (Toner and Catling, 2020). Based on the model predictions, there was no $Na(H_2PO_4)$ minerals precipitation until complete dryness. In prebiotic carbonate-rich lakes (soda ocean), the situation is expected to be closer to our simulations. There, the coupling of evaporative phosphate accumulation and the absence of living organisms, consuming phosphate has been postulated, rendering these water bodies as plausible settings for the origin of life (Toner and Catling, 2020). In a previous work, we have shown that phosphate minerals were absent during the precipitation of $CaCO_3$ mineral vesicles formed by pouring drops of concentrated $CaCl_2$ solution into Lake Magadi brines (Getenet et al., 2020).

Villiaumite (NaF) precipitation was predicted near the final stages of the evaporation process in all samples but wasn't detected by X-ray diffractions probably due to their small amount. However, micrographs of the precipitates revealed rounded cubic crystals of villiaumite between acicular trona crystals obtained from evaporation of Lake Magadi water droplets (Getenet et al., 2022). Villiaumite is a common constituent of the surface deposits of Lake Magadi brines (Baker, 1958; Eugster, 1980). Trona collected from Lake Magadi and Natron, which serves as cooking salt, is reported to also contain kogarkoite or villiaumite (Nielsen, 1999; Nielsen and Dahi, 2002). Fluorite is common in drill cores from southern Lake Natron (Manega and Bieda, 1987). Fluorite in outcrops and core sediments of Lake Magadi and Natron form via redissolution of calcite and/or gaylussite (Eugster, 1980; Surdam and Eugster, 1976) whereas fluorite in efflorescent crusts of the Nasikie Engida hot springs forms due to mixing with relatively Ca-rich dilute water (Renaut et al., 2020).

4.3. Calcium phases

The precipitation of calcite, dolomite, gaylussite and pirssonite in small amounts (<0.5 mmol/kg of brine evaporated) is predicted by our thermodynamic models, but not observed in experiments due to the small amount. Records of these minerals in the stratigraphic sequence are due to the undersaturation–evaporation–supersaturation cycles that tend to concentrate minerals having lower solubility like these. In rainy seasons when freshwater replenishes the lake and supplies additional Ca and Mg, trona, thermonatrite and halite may dissolve, leaving behind the less soluble mineral phases. This cyclic process may have taken place on the lakeshore, accumulating alkaline earth carbonate deposits, and leading to the formation of Lake Magadi brines which are depleted in Ca and Mg and enriched in Na-Cl-CO_3-HCO_3 ions (Eugster, 1980; Eugster, 1970; Jones et al., 1977). Calcite, dolomite, magnesite, gaylussite and pirssonite are present as efflorescent crusts and pisolites in modern sediments and drill cores of Lake Magadi and Nasikie Engida (Eugster, 1986; Eugster, 1980; Renaut et al., 2020; Surdam and Eugster, 1976). Similarly, the core sediments on Lake Natron show interbedded trona and mud with disseminated crystals of calcite, gaylussite and pirssonite. The mid-Pleistocene Peninj sediments contain horizons with dolomite and casts of trona, pirssonite and gaylussite, suggesting that these lacustrine beds were deposited in sodium-carbonate rich lake resembling modern Lake Natron (Hay, 1968; Eugster, 1966; Isaac, 1967;

Manega and Bieda, 1987). Calcite and aragonite precipitation was observed in hydrothermal springs along the shorelines of Lake Natron (Manega and Bieda, 1987). Alkaline earth carbonate and Na—Ca carbonate minerals may form due to the episodic interaction of Ca- and Mg-rich freshwater with Na-rich brine on the lake margins (Eugster, 1980; Owen et al., 2019; Renaut et al., 2020). Alternatively, gaylussite may form via the reaction of Na-rich brines with detrital calcite (Eugster and Hardie, 1978; Surdam and Eugster, 1976). Chert deposits of the Green Beds of Lake Magadi contain open crystal moulds, which are suggested to be calcite, gaylussite or pirssonite (Eugster, 1980; Eugster, 1969; Owen et al., 2019). Eugster (1969) found calcite rosettes in magadiite horizons of the lower High Magadi beds and proposed that they are the source of the carbonate casts. Calcite in these casts may have formed by sodium leaching during the transformation of magadiite to chert (Eugster, 1969). These Ca-Na-carbonate crystals and casts in the chert deposits imply that the paleolake brines may have encountered dilute water with higher Ca concentration (Eugster, 1969; Eugster, 1967; Schubel and Simonson, 1990). This has been supported by the presence of burrows in High Magadi beds (Buatois et al., 2020) and the finding of calcite, Mg-calcite, and dolomite in drill cores of Lake Magadi at depths below 102 m. The cores above 102 m lack calcite or Mg-calcite reflecting the increasing salinity and alkalinity of the paleolake (Owen et al., 2019). Dilution of the brines during events of high freshwater input lowers the phosphate and fluoride content below that of Ca input. In this case, there could be sufficient calcium remaining for calcite, gaylussite and pirssonite to precipitate after fluorite and apatite.

4.4. Silicates and minor phases

The thermodynamic model predicted an initial brine supersaturation with respect to quartz except for Lake Magadi brine which reaches supersaturation in amorphous silica after a CF of 3 (Fig. 5). Silica concentration rises until the initial precipitation of amorphous silica or during the redissolution of amorphous silica and quartz. In Lake Magadi, as the pH rises above 9, silica remains concentrating at the same rate as chloride due to the polymerization of silicic acid (Eugster, 1980, Eugster, 1970; Jones et al., 1977). The control of pH on the precipitation and dissolution of amorphous silica and quartz is clearly visible in the output of the thermodynamic models due to the pH-dependent silica solubility, which dramatically increases beyond pH 8.3 (Krauskopf and Bird, 1979). In our experiments, amorphous silica was detected only in hot spring samples (see Fig. 4c). In Lake Magadi precipitates, it seems that there were visible precipitates without resulting in diffraction peaks, which may indicate the precipitation of amorphous silica (Getenet et al., 2022). In Natron and Nasikie Engida lake brines, neither amorphous silica nor quartz was detected experimentally. Silica gels precipitate in close proximity to the hot springs of Nasikie Engida and near the shorelines under active evaporation (Eugster and Jones, 1968; Renaut et al., 2020; Surdam and Eugster, 1976). A recent study of cherts from drill cores revealed the near-surface synsedimentary formation of Magadi cherts directly from siliceous gels (Leet et al., 2021).

Precipitation of sylvite, glaserite and burkeite is predicted by our model close to complete desiccation. Sylvite was detected by ex-situ X-ray diffractions in all samples and by in-situ diffractions from Lake Natron brine and Nasikie Engida hot spring. However, these phases were not reported in MNN lakes because freshwater supply to the lakes during the rainy season dilutes the brines before they reach supersaturation in sylvite, burkeite and glaserite. However, these minerals have been reported in other alkaline lakes of the East African rift valley, for example, in Lake Katwe (Uganda) (Kasedde et al., 2014; Nielsen, 1999). Borax was predicted to form from the hot spring brine, but not observed in the experiments nor the natural environment of MNN lakes. Borax was reported in other evaporite settings comparable to soda lakes such as the Pleistocene trona deposits of Searles Lake (California) (Smith and Stuiver, 1979).

In summary, the precipitation sequence Ca—Mg carbonates and siliceous sediments, Ca—Na carbonates, Na-carbonates, and halides show the gradual increase of paleolake salinity in geological time scale. A similar precipitation sequence in Lonar Lake (Central India) from calcite through gaylussite to trona was seen during progressive brine evaporation and the onset of drought events in the Holocene (Anoop et al., 2013). The observed and predicted mineral precipitation sequence of Lake Magadi is comparable with the precipitation sequence proposed for the Pleistocene/Holocene evaporites of Searles Lake (USA) (Olson and Lowenstein, 2021).

The impact of biological activity is not included in this model, which may be an additional cause of some differences. For example, bacterial sulphate reduction has been reported to effectively deplete the sulphate content in Lake Magadi (Eugster, 1980, Eugster, 1970; Jones et al., 1977). Hence, the predicted SO_4^{2-} concentration seems higher than the actual ones, explaining the absence of sulphate-containing minerals. Pyrite, found in the drill cores from Lake Magadi (see Owen et al. (2019)), may indicate this sulphate reduction (García-Veigas et al., 2013). Phosphate concentration and precipitation, as discussed above, is also largely controlled by biological activity (Toner and Catling, 2020).

5. Conclusions

In this work, we have determined the mineral precipitation sequence from different rift valley soda lakes and hot spring tributaries to the lakes. Our experiments and calculations show that pH, and consequently CO_3^{2-}/HCO_3^- ratios are the major factors determining the precipitation order, relative quantity, and resulting mineral paragenesis in the East African Rift Valley hyperalkaline, hypersaline lakes and springs. The precipitation of major phases (Na carbonates/bicarbonates) increases the pH of the brines, so the hyperalkaline nature of the lake brines is due to this precipitation while the hypersaline character is due to the high solubility of Na-CO_3^{2-}/HCO_3^- salts.

The sequence of precipitating minerals depends on the starting composition of the brine. In Lake Magadi, Nasikie Engida and Natron, the carbonate alkalinity was dominated by CO_3^{2-} whereas in Nasikie Engida hot spring HCO_3^- was significantly higher than CO_3^{2-}. Nahcolite deposits form only from the northern segment of Nasikie Engida and its feeder hot springs due to the lower pH that makes available enough HCO_3^- for nahcolite precipitation. However, in southern Nasikie Engida, Magadi and Natron lakes, nahcolite precipitates only for a short, transient period during evaporation and re-dissolves when pH increases, leading to the precipitation of trona, which is the main precipitated phase. Thermonatrite and halite form dominantly in local pools and efflorescent crust subjected to intense and fast evaporation that limits the dissolution of atmospheric CO_2. In these conditions, the pH rises significantly after trona and nahcolite precipitation.

Lake brines are rich in Si, which precipitates as silica during the first stages of evaporation at relatively lower pH values but gets redissolved due to the pH increase induced by the precipitation of trona or nahcolite. This redissolution does not happen in the less alkaline waters from the contributing springs. Silica accumulation in the stratigraphic sequence, therefore, requires either low evaporation levels or a relatively lower pH of the brines.

Full range evaporation experiments/simulations up to complete dryness, like the ones presented in this work, show the full landscape of plausible evaporitic scenarios, but only a fraction of this range of conditions is achieved by actual lake brines in perennial lakes. This range of conditions is controlled by the amplitude of seasonal dry/rainy periods, which modulate the balance between the dilution of brines by the inflow of relatively fresh water and the concentration of them by evaporation. The development of hydrochemical models predicting, within this window of conditions, the precipitation sequence, and the relative abundance of evaporitic minerals in the resulting paragenesis is expected to be a novel tool in explaining modern depositional settings and in reconstructing paleoclimatic and hydrochemical conditions during the deposition of ancient evaporite deposits. This approach could also be

adapted to investigate the industrial crystallization of economic minerals from natural brines or even the conditions for the formation of evaporites in extraterrestrial environments using model and analogue brines.

Even though the evaporation rates of the droplets were faster than the lakes, it was slow enough to emulate the precipitation sequences of minerals in the lakes, allowing accurate identification of different anhydrous and hydrated phases. All our experiments and simulations assume that CO_2 diffusion from the atmosphere to the brine is slower than the precipitation/dissolution processes that end-up controlling the pCO_2 value of the brine. This is reasonable for droplets and, more importantly, for the lake and pond surfaces, where fast evaporation occurs. Our results explain the overall precipitation sequence both at the surface and the bottom of lakes but are especially suited for the places where fast evaporation occurs. Therefore, these results are complementary to the previous knowledge obtained from thermodynamic phase calculations, because the pCO_2 values at the bottom of the lake would change much slower, will be less affected by kinetic processes and can be assumed to be adequately described by previous thermodynamic results. Owing to complete dryness, droplet evaporations couldn't reveal back reactions between brine and former precipitated minerals. However, these reactions in the actual lakes are relatively slow processes that can be defined precisely by previous thermodynamic knowledge.

Funding

This work was supported by the European Research Council (grant number 340863); the Spanish Ministerio de Economía y Competitividad via the project CGL2016–78971-P; Junta de Andalucía via the project P18-FR-5008 and the Spanish Ministerio de Ciencia, Innovacion y Universidades (grant number BES-2017-081105) (to M.G.).

Declaration of Competing Interest

The authors declare that they have no known competing financial interests or personal relationships that could have appeared to influence the work reported in this paper.

Data availability

No data was used for the research described in the article.

Acknowledgements

The authors thank Isabel Guerra-Tschuschke for the support during the scanning electron microscopy analyses at the Centro de Instrumentación Científica (CIC) of the University of Granada, Francisca Espinosa, Raquel Fernandez-Penas, Cristóbal Verdugo-Escamilla and Joaquín Criado-Reyes for their technical assistance. We are grateful to Isabel Díaz (Instituto de Catálisis y Petroleoquímica-CSIC) for fluoride analyses. We also thank National Commission for Science Technology and Information, National Environmental Management Authority, and Kenya Wildlife Services for research permissions. Magadi Tata Chemicals Ltd. and National Museums of Kenya provide logistic help. The authors gratefully acknowledge Patricia Gitari, Lukas Sossoika, and Tara Barwa for their assistance in fieldwork.

Appendix A. Supplementary data

Supplementary data to this article can be found online at https://doi.org/10.1016/j.chemgeo.2022.121222.

References

Allen, D.J., Darling, W.G., Burgess, W.G., 1989. Geothermics and hydrogeology of the southern part of the Kenya Rift Valley with emphasis on the Magadi-Nakuru area (No. SD/89/001), British Geological Survey Research Report SD/89/1. In: British Geological Survey Research Report SD/89/1, pp. 1–68.

Anoop, A., Prasad, S., Plessen, B., Basavaiah, N., Gaye, B., Naumann, R., Menzel, P., Weise, S., Brauer, A., 2013. Palaeoenvironmental implications of evaporative gaylussite crystals from Lonar Lake, Central India. J. Quat. Sci. 28, 349–359. https://doi.org/10.1002/jqs.2625.

Baker, B.H., 1958. Geology of the Magadi Area (No. 42), 42. Geol. Surv. Kenya, Nairobi, Kenya, Rep, pp. 81.

Baker, B.H., 1963. Geology of the Area south of Magadi (No. 61), 61. Geol. Surv. Kenya, Nairobi, Kenya, Rep, pp 27.

Baker, B.H., 1986. Tectonics and volcanism of the southern Kenya Rift Valley and its influence on rift sedimentation. Geol. Soc. Lond., Spec. Publ. 25, 45–57. https://doi.org/10.1144/GSL.SP.1986.025.01.05.

Baker, B.H., 1987. Outline of the petrology of the Kenya rift alkaline province. Geol. Soc. Lond., Spec. Publ. 30, 293–311. https://doi.org/10.1144/GSL.SP.1987.030.01.14.

Baker, B.H., Mohr, P.A., Williams, L.A.J., 1972. Geology of the Eastern Rift System of Africa. https://doi.org/10.1130/SPE136-p1.

Behr, H.-J., 2002. Magadiite and Magadi Chert: A Critical Analysis of the Silica Sediments in the Lake Magadi Basin, Kenya. In: Renaut, R.W., Ashley, G.M. (Eds.), Sedimentation in Continental Rifts. SEPM Society for Sedimentary Geology, pp. 257–273. https://doi.org/10.2110/pec.02.73.0257.

Behr, H.-J., Röhricht, C., 2000. Record of seismotectonic events in siliceous cyanobacterial sediments (Magadi cherts), Lake Magadi, Kenya. Int. J. Earth Sci. 89, 268–283. https://doi.org/10.1007/s005319900070.

Bell, K., Dawson, J.B., Farquhar, R.M., 1973. Strontium Isotope Studies of Alkalic Rocks: the active Carbonatite Volcano Oldoinyo Lengai, Tanzania. GSA Bull. 84, 1019–1030. https://doi.org/10.1130/0016-7606(1973)84<1019:SISOAR>2.0.CO;2.

Benecke, G., Wagermaier, W., Li, C., Schwartzkopf, M., Flucke, G., Hoerth, R., Zizak, I., Burghammer, M., Metwalli, E., Müller-Buschbaum, P., Trebbin, M., Förster, S., Paris, O., Roth, S.V., Fratzl, P., 2014. A customizable software for fast reduction and analysis of large X-ray scattering data sets: applications of the new DPDAK package to small-angle X-ray scattering and grazing-incidence small-angle X-ray scattering. J. Appl. Crystallogr. 47, 1797–1803. https://doi.org/10.1107/S1600576714019773.

Bizzarri, B.M., Botta, L., Pérez-Valverde, M.I., Saladino, R., Di Mauro, E., García-Ruiz, J. M., 2018. Silica Metal Oxide Vesicles Catalyze Comprehensive Prebiotic Chemistry. Chem. Eur. J. 24, 8126–8132. https://doi.org/10.1002/chem.201706162.

Blanc, Ph., Lassin, A., Piantone, P., Azaroual, M., Jacquemet, N., Fabbri, A., Gaucher, E. C., 2012. Thermoddem: a geochemical database focused on low temperature water/rock interactions and waste materials. Appl. Geochem. 27, 2107–2116. https://doi.org/10.1016/j.apgeochem.2012.06.002.

Bradley, W.H., Eugster, H.P., 1969. Geochemistry and Paleolimnology of the Trona Deposits and Associated Authigenic Minerals of the Green River Formation of Wyoming (USGS Numbered Series No. Professional Paper 496-B). U.S. Geological Survey.

Buatois, L.A., Renaut, R.W., Owen, R.B., Behrensmeyer, A.K., Scott, J.J., 2020. Animal bioturbation preserved in Pleistocene magadiite at Lake Magadi, Kenya Rift Valley, and its implications for the depositional environment of bedded magadiite. Sci. Rep. 10, 6794. https://doi.org/10.1038/s41598-020-63505-7.

Cabestrero, Ó., Sanz-Montero, M.E., 2018. Brine evolution in two inland evaporative environments: influence of microbial mats in mineral precipitation. J. Paleolimnol. 59, 139–157. https://doi.org/10.1007/s10933-016-9908-0.

Carrozzo, F.G., Sanctis, M.C.D., Raponi, A., Ammannito, E., Castillo-Rogez, J., Ehlmann, B.L., Marchi, S., Stein, N., Ciarniello, M., Tosi, F., Capaccioni, F., Capria, M.T., Fonte, S., Formisano, M., Frigeri, A., Giardino, M., Longobardo, A., Magni, G., Palomba, E., Zambon, F., Raymond, C.A., Russell, C.T., 2018. Nature, formation, and distribution of carbonates on Ceres. Sci. Adv. 4, e1701645 https://doi.org/10.1126/sciadv.1701645.

Dawson, J.B., 1962. The geology of Oldoinyo Lengai. Bull. Volcanol. 24, 349–387. https://doi.org/10.1007/BF02599356.

Dawson, J.B., 1964. Carbonatitic volcanic ashes in Northern Tanganyika. Bull. Volcanol. 27, 81–91. https://doi.org/10.1007/BF02597513.

Dawson, J.B., 2008. The Gregory rift valley and Neogene-recent volcanoes of northern Tanzania, Geological Society of London, Memoirs, 33, 33. Geological Society, London, Memoirs, 102p.

De Cort, G., Mees, F., Renaut, R.W., Sinnesael, M., Van der Meeren, T., Goderis, S., Keppens, E., Mbuthia, A., Verschuren, D., 2019. Late-Holocene sedimentation and sodium carbonate deposition in hypersaline, alkaline Nasikie Engida, southern Kenya Rift Valley. J. Paleolimnol. 62, 279–300. https://doi.org/10.1007/s10933-019-00092-2.

De Sanctis, M.C., Raponi, A., Ammannito, E., Ciarniello, M., Toplis, M.J., McSween, H.Y., Castillo-Rogez, J.C., Ehlmann, B.L., Carrozzo, F.G., Marchi, S., Tosi, F., Zambon, F., Capaccioni, F., Capria, M.T., Fonte, S., Formisano, M., Frigeri, A., Giardino, M., Longobardo, A., Magni, G., Palomba, E., McFadden, L.A., Pieters, C.M., Jaumann, R., Schenk, P., Mugnuolo, R., Raymond, C.A., Russell, C.T., 2016. Bright carbonate deposits as evidence of aqueous alteration on (1) Ceres. Nature 536, 54–57. https://doi.org/10.1038/nature18290.

Demicco, R.V., Lowenstein, T.K., 2019. When “evaporites” are not formed by evaporation: the role of temperature and pCO2 on saline deposits of the Eocene Green River Formation, Colorado, USA. GSA Bull. 132, 1365–1380. https://doi.org/10.1130/B35303.1.

Deocampo, D.M., Renaut, R.W., 2016. Geochemistry of African Soda Lakes. In: Schagerl, M. (Ed.), Soda Lakes of East Africa. Springer International Publishing, Cham, pp. 77–93. https://doi.org/10.1007/978-3-319-28622-8_4.

Earman, S., Phillips, F.M., McPherson, B.J.O.L., 2005. The role of "excess" CO2 in the formation of trona deposits. Appl. Geochem. 20, 2217–2232. https://doi.org/10.1016/j.apgeochem.2005.08.007.
Eugster, H.P., 1966. Sodium carbonate-bicarbonate minerals as indicators of Pco2. J. Geophys. Res. (1896-1977) 71, 3369–3377. https://doi.org/10.1029/JZ071i014p03369.
Eugster, H.P., 1967. Hydrous Sodium Silicates from Lake Magadi, Kenya: Precursors of Bedded Chert. Science 157, 1177–1180. https://doi.org/10.1126/science.157.3793.1177.
Eugster, H.P., 1969. Inorganic bedded cherts from the Magadi area, Kenya. Contrib. Mineral. Petrol. 22, 1–31. https://doi.org/10.1007/BF00388011.
Eugster, H.P., 1970. Chemistry and Origin of the Brines of Lake Magadi, Kenya. Mineral. Soc. Amer. Spec. Pap. 3, 213–235.
Eugster, H.P., 1971. Origin and deposition of trona. Rocky Mountain Geol. 10, 49–55.
Eugster, H.P., 1980. Lake Magadi, Kenya, and its Precursors. In: Nissenbaum, A. (Ed.), Developments in Sedimentology, Hypersaline Brines and Evaporitic Environments. Elsevier, pp. 195–232. https://doi.org/10.1016/S0070-4571(08)70239-5.
Eugster, H.P., 1986. Lake Magadi, Kenya: a model for rift valley hydrochemistry and sedimentation? Geol. Soc. Lond., Spec. Publ. 25, 177–189. https://doi.org/10.1144/GSL.SP.1986.025.01.15.
Eugster, H.P., Hardie, L.A., 1978. Saline Lakes. In: Lerman, A. (Ed.), Lakes: Chemistry, Geology. Physics. Springer, New York, NY, pp. 237–293. https://doi.org/10.1007/978-1-4757-1152-3_8.
Eugster, H.P., Jones, B.F., 1968. Gels Composed of Sodium-Aluminum Silicate, Lake Magadi, Kenya. Science 161, 160–163.
Fritz, B., Zins-Pawlas, M.-P., Gueddari, M., 1987. Geochemistry of silica-rich brines from Lake Natron (Tanzania). Géochimie des saumures riches en silice du lac Natron (Tanzanie). Sciences Géologiques, bulletins et mémoires 40, 97–110. https://doi.org/10.3406/sgeol.1987.1753.
García-Ruiz, J.M., Nakouzi, E., Kotopoulou, E., Tamborrino, L., Steinbock, O., 2017. Biomimetic mineral self-organization from silica-rich spring waters. Sci. Adv. 3, e1602285 https://doi.org/10.1126/sciadv.1602285.
García-Ruiz, J.M., van Zuilen, M.A., Bach, W., 2020. Mineral self-organization on a lifeless planet. Phys Life Rev 34–35, 62–82. https://doi.org/10.1016/j.plrev.2020.01.001.
García-Veigas, J., Gündoğan, İ., Helvacı, C., Prats, E., 2013. A genetic model for Na-carbonate mineral precipitation in the Miocene Beypazarı trona deposit, Ankara province, Turkey. Sediment. Geol. 294, 315–327. https://doi.org/10.1016/j.sedgeo.2013.06.011.
Getenet, M., García-Ruiz, J.M., Verdugo-Escamilla, C., Guerra-Tschuschke, I., 2020. Mineral Vesicles and Chemical Gardens from Carbonate-Rich Alkaline Brines of Lake Magadi, Kenya. Crystals 10, 467. https://doi.org/10.3390/cryst10060467.
Getenet, M., García-Ruiz, J.M., Otálora, F., Emmerling, F., Al-Sabbagh, D., Verdugo-Escamilla, C., 2022. A Comprehensive Methodology for monitoring Evaporitic Mineral Precipitation and Hydrochemical Evolution of Saline Lakes: the Case of Lake Magadi Soda Brine (East African Rift Valley, Kenya). Cryst. Growth Des. 22, 2307–2317. https://doi.org/10.1021/acs.cgd.1c01391.
Giffaut, E., Grivé, M., Blanc, Ph., Vieillard, Ph., Colàs, E., Gailhanou, H., Gaboreau, S., Marty, N., Madé, B., Duro, L., 2014. Andra thermodynamic database for performance assessment: ThermoChimie. In: Applied Geochemistry, Geochemistry for Risk Assessment: Hazardous waste in the Geosphere, 49, pp. 225–236. https://doi.org/10.1016/j.apgeochem.2014.05.007.
Glein, C.R., Baross, J.A., Waite, J.H., 2015. The pH of Enceladus' ocean. Geochim. Cosmochim. Acta 162, 202–219. https://doi.org/10.1016/j.gca.2015.04.017.
Hay, R.L., 1966. Zeolites and Zeolitic Reactions in Sedimentary Rocks, in: Geological Society of America Special Papers. Geological Society of America, pp. 1–122. https://doi.org/10.1130/SPE85-p1.
Hay, R.L., 1968. Chert and its sodium-silicate precursors in sodium-carbonate lakes of East Africa. Contrib. Mineral. Petrol. 17, 255–274. https://doi.org/10.1007/BF00380740.
Hillaire-Marcel, C., Carro, O., Casanova, J., 1986. 14C and Th/U Dating of Pleistocene and Holocene Stromatolites from East African Paleolakes. Quat. Res. 25 https://doi.org/10.1016/0033-5894(86)90004-9, 312–239.
Isaac, G.L., 1965. The stratigraphy of the Peninj Beds and the provenance of the Natron Australopithecine mandible. Quaternaria 7, 101–130.
Isaac, G.L., 1967. The stratigraphy of the Peninj group-early middle Pleistocene formations west of Lake Natron, Tanzania. In: Background to evolution in Africa, pp. 229–257.
Jagniecki, E.A., Lowenstein, T.K., 2015. Evaporites of the Green River Formation, Bridger and Piceance Creek Basins: Deposition, Diagenesis, Paleobrine Chemistry, and Eocene Atmospheric CO2. In: Smith, M.E., Carroll, A.R. (Eds.), Stratigraphy and Paleolimnology of the Green River Formation, Western USA. Syntheses in Limnogeology. Springer Netherlands, Dordrecht, pp. 277–312. https://doi.org/10.1007/978-94-017-9906-5_11.
Jagniecki, E.A., Lowenstein, T.K., Jenkins, D.M., Demicco, R.V., 2015. Eocene atmospheric CO2 from the nahcolite proxy. Geology 43, 1075–1078. https://doi.org/10.1130/G36886.1.
Jones, B.F., Eugster, H.P., Rettig, S.L., 1977. Hydrochemistry of the Lake Magadi basin, Kenya. Geochim. Cosmochim. Acta 41, 53–72. https://doi.org/10.1016/0016-7037(77)90186-7.
Kasedde, H., Kirabira, J.B., Bäbler, M.U., Tilliander, A., Jonsson, S., 2014. Characterization of brines and evaporites of Lake Katwe, Uganda. J. Afr. Earth Sci. 91, 55–65. https://doi.org/10.1016/j.jafrearsci.2013.12.004.
Kempe, S., Kazmierczak, J., 2002. Biogenesis and early Life on Earth and Europa: favored by an Alkaline Ocean? Astrobiology 2, 123–130. https://doi.org/10.1089/153110702753621394.
Kolpakova, M.N., Gaskova, O.L., 2017. Major ions behaviour during evaporation of different saline type water of Western Mongolian lakes (geochemical modelling). Hydrol. Res. 49, 163–176. https://doi.org/10.2166/nh.2017.148.
Kotopoulou, E., Delgado Huertas, A., Garcia-Ruiz, J.M., Dominguez-Vera, J.M., Lopez-Garcia, J.M., Guerra-Tschuschke, I., Rull, F., 2019. A Polyextreme Hydrothermal System Controlled by Iron: the Case of Dallol at the Afar Triangle. ACS Earth Space Chem. 3, 90–99. https://doi.org/10.1021/acsearthspacechem.8b00141.
Krauskopf, K.B., Bird, D.K., 1979. Introduction to Geochemistry. In: International Series in the Earth and Planetary Sciences, 2nd edition. ed. McGraw-Hill.
Lee, H., Muirhead, J.D., Fischer, T.P., Ebinger, C.J., Kattenhorn, S.A., Sharp, Z.D., Kianji, G., 2016. Massive and prolonged deep carbon emissions associated with continental rifting. Nat. Geosci. 9, 145–149. https://doi.org/10.1038/ngeo2622.
Lee, H., Fischer, T.P., Muirhead, J.D., Ebinger, C.J., Kattenhorn, S.A., Sharp, Z.D., Kianji, G., Takahata, N., Sano, Y., 2017. Incipient rifting accompanied by the release of subcontinental lithospheric mantle volatiles in the Magadi and Natron basin, East Africa. J. Volcanol. Geotherm. Res. Volcano-Hydrothermal Syst. 346, 118–133. https://doi.org/10.1016/j.jvolgeores.2017.03.017.
Leet, K., Lowenstein, T.K., Renaut, R.W., Owen, R.B., Cohen, A., 2021. Labyrinth patterns in Magadi (Kenya) cherts: evidence for early formation from siliceous gels. Geology. https://doi.org/10.1130/G48771.1.
Lowenstein, T.K., Demicco, R.V., 2006. Elevated Eocene Atmospheric CO2 and its subsequent Decline. Science 313, 1928. https://doi.org/10.1126/science.1129555.
Lowenstein, T.K., Dolginko, L.A.C., García-Veigas, J., 2016. Influence of magmatic-hydrothermal activity on brine evolution in closed basins: Searles Lake, California. GSA Bull. 128, 1555–1568. https://doi.org/10.1130/B31398.1.
Lowenstein, T.K., Jagniecki, E.A., Carroll, A.R., Smith, M.E., Renaut, R.W., Owen, R.B., 2017. The Green River salt mystery: what was the source of the hyperalkaline lake waters? Earth Sci. Rev. 173, 295–306. https://doi.org/10.1016/j.earscirev.2017.07.014.
Ma, L., Lowenstein, T.K., Russell, J.M., 2011. A Brine Evolution Model and Mineralogy of Chemical Sediments in a Volcanic Crater, Lake Kitagata, Uganda. Aquat. Geochem. 17, 129–140. https://doi.org/10.1007/s10498-010-9108-x.
Manega, P., Bieda, S., 1987. Modern sediments of Lake Natron, Tanzania. Sédimentation récente du lac Natron, Tanzanie. Sciences Géologiques, bulletins et mémoires 40, 83–95. https://doi.org/10.3406/sgeol.1987.1752.
McCord, T.B., Hansen, G.B., Fanale, F.P., Carlson, R.W., Matson, D.L., Johnson, T.V., Smythe, W.D., Crowley, J.K., Martin, P.D., Ocampo, A., Hibbitts, C.A., Granahan, J. C., the NIMS Team, 1998. Salts on Europa's Surface Detected by Galileo's near infrared Mapping Spectrometer. Science 280, 1242–1245. https://doi.org/10.1126/science.280.5367.1242.
McNulty, E., 2017. Lake Magadi and the Soda Lake Cycle: A Study of the Modern Sodium Carbonates and of Late Pleistocene and Holocene Lacustrine Core Sediments (Graduate Dissertations and Theses. 25). Binghamton University, New York, USA.
Nielsen, J.M., 1999. East African magadi (trona): fluoride concentration and mineralogical composition. J. African Earth Sci. Geol. Mineral Resour. East Africa 29, 423–428. https://doi.org/10.1016/S0899-5362(99)00107-4.
Nielsen, J.M., Dahi, E., 2002. Fluoride exposure of East African consumers using alkaline salt deposits known as magadi (trona) as a food preparation aid. Food Addit. Contam. 19, 709–714. https://doi.org/10.1080/02652030210145900.
Olson, K.J., Lowenstein, T.K., 2021. Searles Lake evaporite sequences: Indicators of late Pleistocene/Holocene lake temperatures, brine evolution, and pCO2. GSA Bull. https://doi.org/10.1130/B35857.1.
Otálora, F., Criado-Reyes, J., Baselga, M., Canals, A., Verdugo-Escamilla, C., García Ruiz, J.M., 2020. Hydrochemical and Mineralogical Evolution through Evaporitic Processes in Salar de Llamara Brines (Atacama, Chile). ACS Earth Space Chem. 4, 882–896. https://doi.org/10.1021/acsearthspacechem.0c00085.
Owen, R.B., Renaut, R.W., Muiruri, V.M., Rabideaux, N.M., Lowenstein, T.K., McNulty, E.P., Leet, K., Deocampo, D., Luo, S., Deino, A.L., Cohen, A., Sier, M.J., Campisano, C., Shen, C.-C., Billingsley, A., Mbuthia, A., Stockhecke, M., 2019. Quaternary history of the Lake Magadi Basin, southern Kenya Rift: Tectonic and climatic controls. Palaeogeogr. Palaeoclimatol. Palaeoecol. 518, 97–118. https://doi.org/10.1016/j.palaeo.2019.01.017.
Paris, O., Li, C., Siegel, S., Weseloh, G., Emmerling, F., Riesemeier, H., Erko, A., Fratzl, P., 2007. A new experimental station for simultaneous X-ray microbeam scanning for small- and wide-angle scattering and fluorescence at BESSY II. J. Appl. Crystallogr. 40, s466–s470. https://doi.org/10.1107/S0021889806045444.
Parkhurst, D.L., Appelo, C.A.J., 2013. Description of input and examples for PHREEQC version 3: A computer program for speciation, batch-reaction, one-dimensional transport, and inverse geochemical calculations (Report No. 6-A43). In: Techniques and Methods. Reston, VA. https://doi.org/10.3133/tm6A43.
Pecoraino, G., D'Alessandro, W., Inguaggiato, S., 2015. The Other Side of the Coin: Geochemistry of Alkaline Lakes in Volcanic areas. In: Rouwet, D., Christenson, B., Tassi, F., Vandemeulebrouck, J. (Eds.), Volcanic Lakes, Advances in Volcanology. Springer, Berlin, Heidelberg, pp. 219–237. https://doi.org/10.1007/978-3-642-36833-2_9.
Reinhardt, M., Goetz, W., Duda, J.-P., Heim, C., Reitner, J., Thiel, V., 2019. Organic signatures in Pleistocene cherts from Lake Magadi (Kenya) – implications for early Earth hydrothermal deposits. Biogeosciences 16, 2443–2465. https://doi.org/10.5194/bg-16-2443-2019.
Renaut, R.W., Owen, R.B., Lowenstein, T.K., Cort, G.D., Mcnulty, E., Scott, J.J., Mbuthia, A., 2020. The role of hydrothermal fluids in sedimentation in saline alkaline lakes: evidence from Nasikie Engida, Kenya Rift Valley. Sedimentology 68, 108–134. https://doi.org/10.1111/sed.12778.
Rull, F., Guerrero, J., Venegas, G., Gázquez, F., Medina, J., 2014. Spectroscopic Raman study of sulphate precipitation sequence in Rio Tinto mining district (SW Spain).

Environ. Sci. Pollut. Res. 21, 6783–6792. https://doi.org/10.1007/s11356-013-1927-z.

Saladino, R., Botta, G., Bizzarri, B.M., Di Mauro, E., Garcia Ruiz, J.M., 2016. A Global Scale Scenario for Prebiotic Chemistry: Silica-based Self-Assembled Mineral Structures and Formamide. Biochemistry 55, 2806–2811. https://doi.org/10.1021/acs.biochem.6b00255.

Schagerl, M., Renaut, R.W., 2016. Dipping into the Soda Lakes of East Africa. In: Schagerl, M. (Ed.), Soda Lakes of East Africa. Springer International Publishing, Cham, pp. 3–24. https://doi.org/10.1007/978-3-319-28622-8_1.

Schubel, K.A., Simonson, B.M., 1990. Petrography and diagenesis of cherts from Lake Magadi, Kenya. J. Sediment. Res. 60, 761–776. https://doi.org/10.1306/212F9269-2B24-11D7-8648000102C1865D.

Smith, G.I., Stuiver, M., 1979. Subsurface stratigraphy and geochemistry of late Quaternary evaporites, Searles Lake, California, with a section on radiocarbon ages of stratigraphic units (Report No. 1043), Professional Paper. In: U.S. Geological Survey Professional Paper 1043. https://doi.org/10.3133/pp1043, 130 p.

Smith, M.E., Carroll, A.R., 2015. Introduction to the Green River Formation. In: Smith, M.E., Carroll, A.R. (Eds.), Stratigraphy and Paleolimnology of the Green River Formation, Western USA, Syntheses in Limnogeology. Springer, Netherlands, Dordrecht, pp. 1–12. https://doi.org/10.1007/978-94-017-9906-5_1.

Surdam, R.C., Eugster, H.P., 1976. Mineral reactions in the sedimentary deposits of the Lake Magadi region, Kenya. GSA Bull. 87, 1739–1752. https://doi.org/10.1130/0016-7606(1976)87<1739:MRITSD>2.0.CO;2.

Toner, J.D., Catling, D.C., 2020. A carbonate-rich lake solution to the phosphate problem of the origin of life. PNAS 117, 883–888. https://doi.org/10.1073/pnas.1916109117.

Wolf, S.E., Leiterer, J., Kappl, M., Emmerling, F., Tremel, W., 2008. Early Homogenous Amorphous Precursor Stages of Calcium Carbonate and subsequent Crystal Growth in Levitated Droplets. J. Am. Chem. Soc. 130, 12342–12347. https://doi.org/10.1021/ja800984y.